

Towards Fair and Robust Volumetric CT Classification via KL-Regularised Group Distributionally Robust Optimisation

Samuel Johnny¹, Blessed Guda², Frank Ebeledike¹, Goodness Obasi¹, Moise Busogi¹

¹Carnegie Mellon University Africa, Kigali, Rwanda

²Carnegie Mellon University, Pittsburgh, USA

{sjohnny,blessedg febeledi, gobasi, mbusogi}@andrew.cmu.edu

Abstract

*Automated diagnosis from chest computed tomography (CT) scans faces two persistent challenges in clinical deployment: distribution shift across acquisition sites, and performance disparity across demographic subgroups. We address both simultaneously across two complementary tasks: binary COVID-19 classification from multi-site CT volumes (Task 1) and four-class lung pathology recognition with gender-based fairness constraints (Task 2). Our framework combines a lightweight MobileViT-XXS slice encoder with a two-layer SliceTransformer aggregator for volumetric reasoning, and trains with a KL-regularised Group Distributionally Robust Optimisation (Group DRO) objective that adaptively upweights underperforming acquisition centres and demographic subgroups. Unlike standard Group DRO, the KL penalty prevents group weight collapse, providing a stable balance between worst-case protection and average performance. For Task 2, we define groups at the granularity of gender \times class, directly targeting severely underrepresented combinations such as female Squamous cell carcinoma. On Task 1, our best configuration achieves a challenge F1 of **0.835**, surpassing the best published challenge entry by +5.9. On Task 2, Group DRO with $\alpha = 0.5$ achieves a mean per-gender macro F1 of **0.815**, outperforming the best challenge entry by +11.1 pp and improving Female Squamous F1 by +17.4 over the Focal Loss baseline.*

1. Introduction

Early detection of diseases such as COVID-19 and primary lung carcinomas from computed tomography (CT) scans has attracted significant research attention, owing to the potential for scalable, automated clinical screening [12–14]. While early approaches treated each CT volume as a collection of independent 2D axial slices, this discards the inter-slice spatial context that is often critical for diagnosis [15].

More recent methods process the full 3D volume directly, though this incurs substantial computational cost. A practical middle ground is to encode slices independently with a shared 2D backbone and then aggregate the resulting representations into a single volumetric descriptor, preserving spatial context at manageable cost.

Despite their promise, CT-based classifiers face two persistent challenges when deployed in real clinical settings. First, *domain shift*: scans acquired across different hospitals vary in scanner hardware, reconstruction kernels, and imaging protocols, causing models trained on one site to generalise poorly to others [6]. Second, *demographic fairness*: class distributions are rarely balanced across patient subgroups such as gender, and standard training objectives optimise average performance at the expense of underrepresented groups. These issues are especially pronounced in small, multi-centre datasets, where existing domain generalisation methods, typically designed for large-scale settings, offer limited benefit [7, 28].

In this work, we address both challenges simultaneously through a group-aware training objective applied to two related tasks: binary COVID-19 classification across four acquisition centres (*Task 1*), and four-class lung pathology classification with gender-based fairness constraints (*Task 2*) [14, 17]. We build on Group Distributionally Robust Optimisation (Group DRO) [22], which minimises the worst-case loss over predefined subgroups rather than the average loss, and augment it with a KL regularisation term that prevents the group weights from collapsing onto a single hard group. This KL-regularised Group DRO objective provides a principled mechanism for reweighting underrepresented subgroups such as female Squamous cell carcinoma patients (5 training samples), without discarding information from majority groups.

Our framework is built on a lightweight MobileViT-XXS slice encoder [21] paired with a two-layer SliceTransformer aggregator, keeping the total parameter count under 1.3M and making the approach practical for small clinical datasets. In summary, our contributions are:

1. A volumetric CT classification framework combining a MobileViT-XXS slice encoder with a SliceTransformer aggregator, achieving competitive performance at under 2M parameters on both single-site and multi-centre benchmarks.
2. A KL-regularised Group DRO training objective that adaptively reweights acquisition centres (*Task 1*) and fine-grained gender×class subgroups (*Task 2*), improving worst-case subgroup performance over standard weighted cross-entropy and Focal Loss baselines [20].
3. Systematic ablation of the KL regularisation strength α and aggregator design, providing actionable insights for practitioners working with small, demographically imbalanced medical imaging datasets.

2. Related Work

2.1. CT-based Disease Classification

Automated analysis of chest CT scans for disease detection has been an active area of research, driven by the clinical need for scalable screening tools. Early approaches processed CT volumes as independent collections of 2D axial slices, applying standard convolutional neural networks to each slice before aggregating predictions via majority voting or simple pooling [1, 2, 9, 24]. While computationally efficient, these methods discard inter-slice spatial context that is often critical for distinguishing pathologies with characteristic 3D distributions, such as ground-glass opacities in COVID-19 [12, 25].

The emergence of large-scale CT datasets has enabled more sophisticated volumetric approaches. Kollias et al. [13] introduced the AI-MIA framework for COVID-19 detection and severity grading, demonstrating that 3D-aware architectures outperform slice-level baselines when sufficient training data is available. Subsequent work extended this to multi-source settings, combining CT with clinical metadata and achieving improved generalisation across multiple data centres [6, 14]. More recently, vision-language models have been explored for CT segmentation and detection, leveraging large pretrained representations to reduce the annotation burden [16]. Our work builds on this line of research but focuses on the under-explored regime of small, multi-centre datasets where volumetric encoders must be both lightweight and distribution-aware.

2.2. Domain Generalisation in Medical Imaging

Distribution shift across data centers is one of the most persistent challenges in clinical AI deployment. Scanners from different manufacturers, varying reconstruction kernels, and institutional imaging protocols all contribute to covariate shift that degrades model performance when evaluated on unseen domains [7, 17, 26]. Guan and Liu [7] provide a comprehensive survey of domain adaptation techniques for

medical imaging, cataloguing approaches ranging from adversarial feature alignment to self-supervised pretraining. The survey showed that most methods require either large multi-site training sets or access to target domain data at test time.

Data augmentation strategies have been proposed to simulate domain diversity during training. Zhang et al. [28] demonstrate that stacking domain-randomised transformations can improve generalisation to unseen sites for segmentation tasks, but find that performance degrades significantly when the training set is small and lacks site diversity [28, 30]. This limitation is particularly acute in our setting, where the training data comprises fewer than 1,300 volumes across four centres with highly unequal class distributions. Rather than augmenting the input space, we address distribution shift directly in the objective function via group-level loss reweighting, which does not require additional data or target domain samples.

2.3. Distributionally Robust Optimisation

Distributionally Robust Optimisation (DRO) provides a principled framework for training models that perform well under worst-case distributional shifts [5, 22, 23]. Group DRO, introduced by Sagawa et al. [22], minimises the maximum expected loss over a set of predefined groups, rather than the average loss across all samples. Group weights are updated by exponentiated gradient ascent, upweighting groups with high loss at each training step. Empirically, Group DRO has been shown to substantially reduce worst-case subgroup error on benchmark datasets, though the authors note that strong ℓ_2 regularisation is necessary to prevent overfitting on small minority groups.

Follow-up work has applied DRO to long-tail recognition, fairness in face recognition and medical imaging fairness [17]. Kollias et al. [17] specifically address multi-source and demographic fairness in disease diagnosis, demonstrating that group-aware objectives improve per-subgroup performance on CT-based tasks. Our work extends this line by introducing a KL regularisation term toward the uniform group weight distribution, which prevents the group weights from collapsing onto a single hard group, a failure mode observed at high DRO learning rates on small datasets. Furthermore, we define groups at the finer granularity of gender×class for *Task 2*, directly targeting underrepresented combinations such as female Squamous cell carcinoma (5 training samples) that would otherwise be subsumed by majority group gradients.

2.4. Lightweight Vision Transformers for Medical Imaging

The Vision Transformer (ViT) [4] and its descendants have demonstrated strong performance on the image classification benchmarks, but their quadratic attention com-

plexity, large parameter count, and large data size make them impractical for resource-constrained medical imaging pipelines. MobileViT [21] addresses this by interleaving standard MobileNet convolution blocks with local Transformer blocks, achieving competitive accuracy at a fraction of the parameters of standard ViT models. The XXS variant used in our work contains approximately 1.3M parameters in the backbone, making it well-suited for small dataset regimes where large models are prone to overfitting.

Several recent works have adapted lightweight transformers for medical imaging [3, 8, 18, 19, 27, 29]. Kollias et al. [15] propose a deep neural architecture that harmonises 3D input analysis with decision making, demonstrating that compact architectures with task-specific aggregation outperform heavier general-purpose models when training data is limited [10, 11]. Similarly, SAM2CLIP2SAM [16] proposes a vision-language pipeline for 3D CT segmentation in which a Segment Anything Model (SAM) first delineates candidate lung regions, CLIP provides semantic grounding of the segmented regions, and a second SAM pass refines the final segmentation masks for COVID-19 detection. While this approach leverages powerful pretrained vision-language representations to reduce annotation dependence, it is designed for segmentation, which introduces an overhead that may not be needed for this data. It also does not address distribution shift across different groups. Our SliceTransformer aggregator follows this philosophy: rather than processing the full 3D volume with a volumetric backbone, we apply a shared 2D encoder to each slice and use a lightweight two-layer Transformer Encoder to aggregate slice-level features. This design keeps the total parameter count low while capturing long-range inter-slice dependencies that are simple pooling aggregators miss.

3. Method

3.1. Overview

Our framework addresses volumetric CT classification under two forms of distribution shift: acquisition-site heterogeneity across four hospitals (Task 1) and demographic imbalance across gender and class combinations (Task 2). The pipeline consists of three components: a slice-level visual encoder, a volumetric aggregator, and a domain-robust training objective. Given a 3D CT volume, the model produces a class prediction of presence or absence of Covid-19 in a single forward pass, without test-time adaptation or site-specific normalisation.

3.2. Problem Formulation

Let $\mathcal{D} = \{(\mathbf{X}_i, y_i, g_i)\}_{i=1}^N$ denote a dataset of CT volumes, where $\mathbf{X}_i \in \mathbb{R}^{1 \times S \times H \times W}$, $y_i \in \mathcal{Y}$ is the class label, and $g_i \in \mathcal{G}$ is a group identifier. For Task 1, $\mathcal{G} = \{0, 1, 2, 3\}$ indexes the four acquisition centres; for Task 2,

$\mathcal{G} = \{0, \dots, 7\}$ indexes the $|\text{gender}| \times |\mathcal{Y}| = 2 \times 4$ sub-groups.

Standard Empirical Risk Minimisation (ERM) minimises the average loss $\frac{1}{N} \sum_i \ell(\mathbf{X}_i, y_i)$, which can yield models that perform well in aggregate while failing on minority groups [22]. We instead optimise for the worst-case group loss:

$$\min_{\theta} \max_{g \in \mathcal{G}} \mathbb{E}_{(\mathbf{X}, y) \sim \mathcal{D}_g} [\ell_{\theta}(\mathbf{X}, y)]. \quad (1)$$

In the task, our model learns to predict the presence or absence of COVID-19 given the CT scan of a subject.

3.3. Model Architecture

The overall pipeline of the proposed method is illustrated in Figure 1; each component is described in detail in the following paragraphs.

Slice encoder. Each axial slice $\mathbf{x}_s \in \mathbb{R}^{1 \times H \times W}$ is processed independently by a shared MobileViT-XXS backbone [21]. MobileViT-XXS combines lightweight MobileNet convolutions with local Transformer blocks, yielding a strong feature extractor at only $\sim 3.42\text{M}$ parameters. The original RGB stem is adapted to single-channel input by averaging the pretrained convolutional weights across the channel dimension, preserving pretrained representations. With the classification head removed, the backbone produces a slice-level embedding $\mathbf{f}_s = \text{Enc}(\mathbf{x}_s) \in \mathbb{R}^d$, where $d = 320$.

SliceTransformer Aggregator The $S = 64$ per-slice embeddings are stacked into a sequence $\mathbf{F} = [\mathbf{f}_1, \dots, \mathbf{f}_S] \in \mathbb{R}^{S \times d}$ and passed through a two-layer Transformer Encoder with $d_{\text{ff}} = 4d$ and 4 attention heads. Global mean pooling over the sequence dimension yields a volume-level representation $\mathbf{z} \in \mathbb{R}^d$. Self-attention over the slice dimension allows the aggregator to learn which anatomical levels carry the strongest diagnostic signal, rather than treating all slices equally which could hurt the learning.

Classification head. The volume-level representation $\mathbf{z} \in \mathbb{R}^d$ is passed through a linear classifier preceded by Layer-Norm and Dropout ($p=0.3$). For *Task 1*, the head produces two logits (COVID / non-COVID); For *Task 2*, it produces four logits corresponding to Adenocarcinoma, Squamous cell carcinoma, COVID-19, and Healthy. In both cases, class probabilities are obtained by applying softmax to the output logits of the linear head.

3.4. Domain-Robust Training

Group DRO with KL regularisation. We solve the minimax objective in Eq. (1) via the exponentiated gradient update of [22]. Group weights $\{w_g\}$ are initialised to uniform

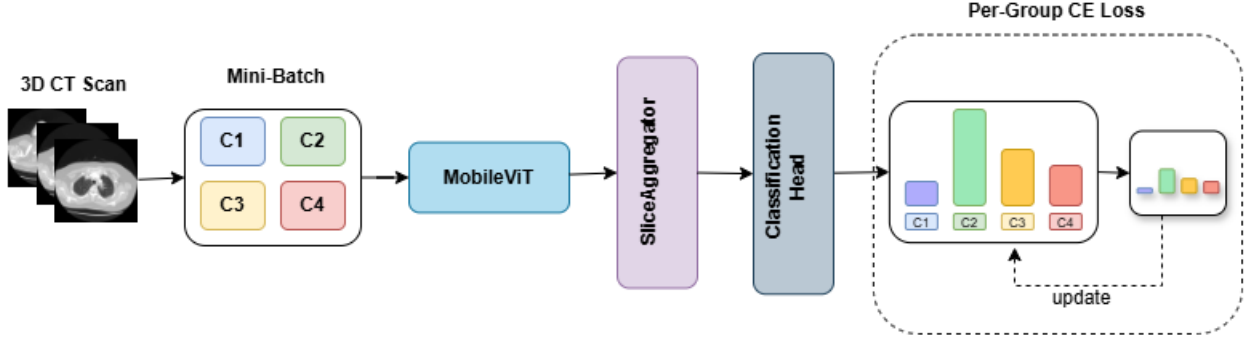


Figure 1. Overview of the proposed pipeline. A 3D CT scan is split into 64 slices, each encoded independently by a shared MobileViT backbone. A learned SliceAggregator pools slice features via attention weighting. The Classification Head produces predictions per sample, and Group DRO with KL regularization dynamically reweights per-centre losses during training.

$w_g = 1/|\mathcal{G}|$ and updated each mini-batch:

$$w_g \leftarrow \frac{w_g \cdot \exp(\eta_{\text{dro}} \cdot \ell_g)}{\sum_{g'} w_{g'} \cdot \exp(\eta_{\text{dro}} \cdot \ell_{g'})}, \quad (2)$$

where $\eta_{\text{dro}} = 0.01$ is the DRO step size. Groups absent from a mini-batch contribute $\ell_g = 0$, so their weights decay passively through renormalisation. The group losses ℓ_g in the weight update are detached from the computation graph; only \mathcal{L} in Eq. (3) provides gradients to model parameters. To prevent weight collapse onto a single hard group, we add a KL penalty toward the uniform distribution:

$$\mathcal{L} = \sum_{g \in \mathcal{G}} w_g \ell_g + \alpha \cdot D_{\text{KL}}(\mathbf{w} \parallel \mathbf{u}), \quad (3)$$

where \mathbf{u} is the uniform distribution over groups and $\alpha \geq 0$ controls regularisation strength. Setting $\alpha = 0$ recovers standard *vanilla* Group DRO; large α forces equal group weighting, recovering empirical risk minimization(ERM).

Group definitions. For *Task 1*, each group $g \in \{0, 1, 2, 3\}$ corresponds to an acquisition centre, directly matching the challenge evaluation metric. For *Task 2*, each group $g = 2j + k$ is the joint index of gender $j \in \{0, 1\}$ (male/female) and class $k \in \{0, 1, 2, 3\}$ (Adenocarcinoma, Squamous, COVID-19, Healthy), yielding $|\mathcal{G}| = 8$ groups. This fine-grained grouping explicitly upweights underrepresented gender-class combinations such as Female Squamous cell carcinoma (in *Task 2*), which would otherwise be dominated by the loss on majority classes.

4. Experiments

4.1. Datasets

Task 1: Multi-Source COVID-19 Detection This task includes CT volumes collected from four hospitals and medical centres (centres 0-3). The dataset comprises 1,530 volumes (train: 1,222; val: 308; test: held out), with 659 non-COVID and 564 COVID-positive cases in the training split. Each volume is labelled binary (COVID / non-COVID) and annotated with a centre identifier $g \in \{0, 1, 2, 3\}$. The challenge metric is the average macro F1 across all four centres:

$$P = \frac{1}{4} \sum_{i=0}^3 \frac{F1_{\text{covid}}^i + F1_{\text{non-covid}}^i}{2} \quad (4)$$

Task 2: Fair Disease Diagnosis CT volumes are labelled across four classes: Adenocarcinoma (A), Squamous cell carcinoma (G), COVID-19, and Healthy (normal). The dataset comprises 889 volumes (train: 734; val: 155) with notable class imbalance: female Squamous has only 5 training samples vs. 125 for female Adenocarcinoma. Each sample carries a gender label (male/female) in addition to the class label. The evaluation metric is the mean per-gender macro F1.

$$P = \frac{1}{2} (F1_{\text{male}}^{\text{macro}} + F1_{\text{non-female}}^{\text{macro}}) \quad (5)$$

4.2. Implementation Details

All models use MobileViT-XXS pretrained on ImageNet-1k. Input volumes are resampled to $S = 64$ slices at 224×224 pixels. We used a batch size of 8 volumes; the

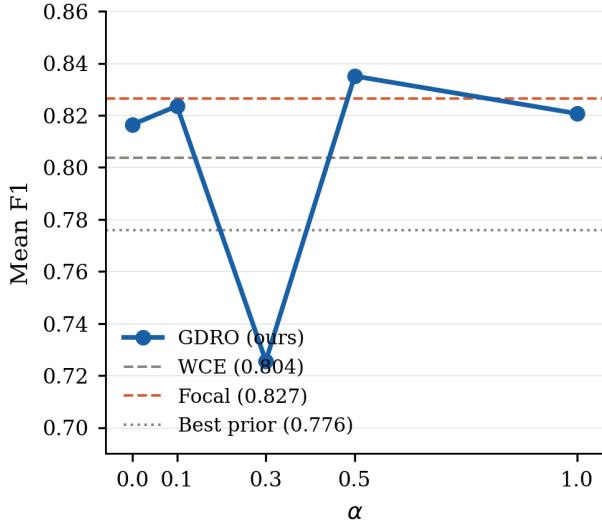


Figure 2. Effect of KL regularisation strength α on Task 2 validation performance, reported separately for male and female sub-groups. Group DRO with $\alpha = 0.5$ achieves the best mean F1 of 0.815 and the smallest gender gap, outperforming Focal Loss (0.804) and the best published challenge entry (0.776 [17]). At $\alpha = 1.0$, male macro rises while female macro falls sharply, indicating that forcing uniform weights over-regularises the minority gender sub-group.

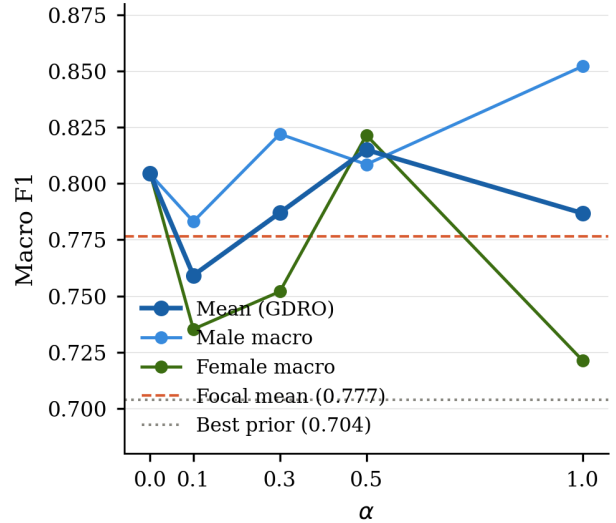


Figure 3. Effect of KL regularisation strength α on Task 1 validation performance. Group DRO with $\alpha = 0.5$ achieves the best mean F1 of 0.835, surpassing both the weighted CE baseline (0.804) and the best published challenge entry (0.776 [17]). Large α forces uniform group weights, collapsing toward ERM and degrading performance ($\alpha = 0.3$, F1 = 0.726).

4.3. Task 1: Multi-Source COVID-19 Detection

Quantitative comparison. Table 1 reports per-centre F1 and overall challenge score P across all configurations and prior work. Group DRO with $\alpha = 0.5$ achieves the best overall F1 of **0.835**, outperforming weighted CE by +3.1 Focal Loss by +0.8 and the best published challenge entry (FDVTS, 0.776) by +5.9.

Effect of KL regularisation. Figure 3 shows the full α sweep. Setting $\alpha = 0.0$ (plain Group DRO) already improves over both baselines, confirming the value of group-aware training even without regularisation. A small KL penalty ($\alpha = 0.1$) provides a further gain, while $\alpha = 0.3$ degrades sharply to 0.726 consistent with the KL term over-constraining group weight dynamics and collapsing toward ERM behaviour. The optimal $\alpha = 0.5$ sits at the balance point between worst-case protection and average performance stability, a pattern that holds on Task 2 as well, suggesting it is a robust hyperparameter choice for small multi-site medical datasets.

Centre 2 domain shift. Centre 2 exhibits near-zero COVID F1 across *all* configurations (Table 1). Every method produces near-zero COVID F1 for Centre 2 while centres 0, 1, and 3 each exceed 0.84. This persistent failure is consistent with a severe single-centre acquisition shift is likely a distinct scanner model, reconstruction kernel,

Method	C0	C1	C2	C3	$P \uparrow$
<i>Prior work</i>					
ACVLAB [18]	0.952	0.742	0.512	0.909	0.779
FDVTS [27]	0.962	0.729	0.490	0.921	0.776
PHAROS Baseline [17]	70.1	85.8	65.3	44.2	85.1
<i>Ours</i>					
WCE	0.920	0.841	0.489	0.965	0.804
Focal ($\gamma=2$)	0.920	<u>0.943</u>	0.489	0.954	<u>0.827</u>
GDRO $\alpha=0.0$	0.909	0.920	0.483	0.954	0.817
GDRO $\alpha=0.1$	0.943	0.909	0.477	0.965	0.824
GDRO $\alpha=0.5$	0.920	0.955	0.489	0.977	0.835

Table 1. Task 1 results and comparison with prior work [17]. Per-centre macro F1 and overall $P \uparrow$. **Bold** = best; u = second best.

SliceTransformer processes $8 \times 64 = 512$ slice embeddings per step. Training uses AdamW ($\beta_1 = 0.9$, $\beta_2 = 0.999$, weight decay 10^{-4}) with a cosine schedule and a 5-step linear warm-up and an initial learning rate 10^{-4} unless stated otherwise. All experiments are conducted on a single NVIDIA L40S GPU. Early stopping monitors validation loss with a patience of 10 epochs.

Configuration	Loss	Male					Female					Mean F1 \uparrow
		A \uparrow	G \uparrow	Cv \uparrow	No \uparrow	Mac. \uparrow	A \uparrow	G \uparrow	Cv \uparrow	No \uparrow	Mac. \uparrow	
<i>Prior work</i>												
FDVTS [19]	-	-	-	-	-	62.5	-	-	-	-	78.3	70.4
PHAROS Baseline [17]	-	-	-	-	-	55.9	-	-	-	-	68.7	62.3
<i>Ours</i>												
Weighted CE	WCE	0.8462	0.6364	0.8500	0.8500	0.7956	0.8136	0.2500	0.9524	0.9231	0.7348	0.7652
Focal ($\gamma=2$)	FL	0.7660	0.6429	0.9000	0.8718	0.7952	0.7200	0.4615	0.9268	0.9231	0.7579	0.7765
<i>Group DRO (α sweep)</i>												
$\alpha=0.0$	GDRO	0.8000	0.6667	0.9000	0.8500	0.8042	0.8421	0.5263	0.9268	0.9231	0.8046	0.8044
$\alpha=0.1$	GDRO	0.8235	0.6087	0.8500	0.8500	0.7831	0.7667	0.3333	0.9524	0.8889	0.7353	0.7592
$\alpha=0.3$	GDRO	0.8889	0.7000	0.8571	0.8421	0.8220	0.8333	0.3750	0.9048	0.8947	0.7520	0.7870
$\alpha=0.5$	GDRO	0.8679	0.6667	0.8421	0.8571	0.8085	0.8519	0.6364	0.9091	0.8889	0.8215	0.8150
$\alpha=1.0$	GDRO	0.8936	0.8148	0.8500	0.8500	0.8521	0.7719	0.3158	0.9091	0.8889	0.7214	0.7868

Table 2. Task 2 results and comparison with prior work. Per-class F1 for each gender group (**A** = Adenocarcinoma, **G** = Squamous, **Cv** = COVID-19, **No** = Normal), per-gender macro F1, and mean across genders (challenge metric \uparrow). Prior work Mean F1 reported in % from the challenge report [17]; ours in decimal. **Bold** = best per column.

or imaging protocol, that produces a distribution not represented in any other training site. Group DRO addresses imbalanced loss across known groups, but it cannot recover signal from a distribution that was never observed during training. This result highlights a fundamental limitation of reweighting-based approaches that we intend to address in future work via test-time adaptation.

4.4. Task 2: Fair Disease Diagnosis

Quantitative comparison. Table 2 reports per-class and per-gender F1 across all configurations. Group DRO with $\alpha = 0.5$ achieves the best mean per-gender macro F1 of **0.815**, outperforming Focal Loss and the weighted CE baseline, and surpassing the best challenge entry (FDVTS, 70.4%). Gains are consistent across both gender groups: male macro F1 improves from 0.795 (Focal) to 0.809, and female macro from 0.758 to 0.822.

Effect of KL regularisation. Figure 2 shows the full α sweep, reported separately for male and female subgroups. Without regularisation ($\alpha = 0.0$), Group DRO already outperforms both baselines. Increasing α to 0.5 yields the best mean F1 and the smallest gender gap ($\Delta = 0.013$), suggesting the KL penalty suppresses weight collapse onto the hardest group without sacrificing minority performance. At $\alpha = 1.0$, male macro rises to 0.852 while female macro falls to 0.721, an artefact of forcing weights toward uniformity, which disproportionately benefits majority subgroups and reduces the targeted upweighting of Female Squamous.

Fine-grained group formulation. The 8-group (gender \times class) formulation is central to the Task 2 result. A coarser 2-group (gender-only) design would conflate the female-Squamous subgroup with the much larger female-Adenocarcinoma group (125 samples), preventing targeted upweighting of the most underrepresented combination. The improvement in Female-G F1 from 0.462 (Focal Loss) to 0.636 (GDRO $\alpha=0.5$) is the clearest evidence that fine-grained grouping, not simply better average optimisation, drives the performance gain on the minority subgroup.

5. Conclusion

We presented a domain-robust and fairness-aware framework for volumetric CT classification, combining a lightweight MobileViT-XXS slice encoder with a Slice-Transformer aggregator and a KL-regularised Group DRO training objective. On Task 1 (COVID-19, four acquisition centres), our best configuration achieves a challenge F1 of **0.835**, outperforming the best published challenge entry by +5.9 pp. On Task 2 (four-class lung pathology with gender fairness constraints), Group DRO with $\alpha=0.5$ achieves a mean per-gender macro F1 of **0.815**, surpassing the best challenge entry and improving Female Squamous F1 over the Focal Loss baseline.

The persistent failure on Centre 2 in *Task 1* highlights that reweighting-based approaches cannot compensate for domains that are absent from training data. Future work will explore test-time adaptation and site-specific normalisation as complementary strategies for this failure

mode. Looking ahead, a natural direction for this work is model compression toward deployment on lower-powered edge devices, such as point-of-care scanners and portable imaging units common in resource-constrained clinical settings.

References

- [1] Ebtesam Al-Mansor, Mohammed Al-Jabbar, Anis Ben Ishak, and S. Abdel-Khalek. Medical image edge detection in the framework of quantum representations. *Alexandria Engineering Journal*, 81:234–242, 2023. 2
- [2] Anastasios Arsenos, Dimitrios Kollias, and Stefanos Kollias. A large imaging database and novel deep neural architecture for covid-19 diagnosis. In *2022 IEEE 14th Image, Video, and Multidimensional Signal Processing Workshop (IVMSP)*, page 1–5. IEEE, 2022. 2
- [3] Wen-Ling Chou, Guo-Shiang Lin, Ku-Yaw Chang, Sheng-Lei Yan, and Wei-Cheng Yeh. Light-weight vision transformer-based semantic segmentation for medical images. In *2025 IEEE International Conference on Advanced Visual and Signal-Based Systems (AVSS)*, pages 1–4, 2025. 3
- [4] Alexey Dosovitskiy, Lucas Beyer, Alexander Kolesnikov, Dirk Weissenborn, Xiaohua Zhai, Thomas Unterthiner, Mostafa Dehghani, Matthias Minderer, Georg Heigold, Sylvain Gelly, Jakob Uszkoreit, and Neil Houlsby. An image is worth 16x16 words: Transformers for image recognition at scale. In *International Conference on Learning Representations (ICLR)*, 2021. 2
- [5] Peyman Mohajerin Esfahani and Daniel Kuhn. Data-driven distributionally robust optimization using the wasserstein metric. *Mathematical Programming*, 171:115–166, 2018. 2
- [6] Demetris Gerogiannis, Anastasios Arsenos, Dimitrios Kollias, Dimitris Nikitopoulos, and Stefanos Kollias. Covid-19 computer-aided diagnosis through ai-assisted ct imaging analysis: Deploying a medical ai system. In *2024 IEEE International Symposium on Biomedical Imaging (ISBI)*, pages 1–4. IEEE, 2024. 1, 2
- [7] Hao Guan and Mingxia Liu. Domain adaptation for medical image analysis: A survey. *IEEE Transactions on Biomedical Engineering*, 69(3):1173–1185, 2022. 1, 2
- [8] B. Huang, Y. Liu, B. Tang, et al. Inceptionmamba: A lightweight and effective model for medical image classification revealing mamba’s low-frequency bias. *Neural Processing Letters*, 58(15), 2026. 3
- [9] Dimitrios Kollias, Athanasios Tagaris, Andreas Stafylopatis, Stefanos Kollias, and Georgios Tagaris. Deep neural architectures for prediction in healthcare. *Complex & Intelligent Systems*, 4(2):119–131, 2018. 2
- [10] Dimitrios Kollias, N Bouas, Y Vlaxos, V Brillakis, M Seferis, Ilianna Kollia, Levon Sukissian, James Wingate, and S Kollias. Deep transparent prediction through latent representation analysis. *arXiv preprint arXiv:2009.07044*, 2020. 3
- [11] Dimitris Kollias, Y Vlaxos, M Seferis, Ilianna Kollia, Levon Sukissian, James Wingate, and Stefanos D Kollias. Transparent adaptation in deep medical image diagnosis. In *TAILOR*, page 251–267, 2020. 3
- [12] Dimitrios Kollias, Anastasios Arsenos, Levon Soukissian, and Stefanos Kollias. Mia-cov19d: Covid-19 detection through 3-d chest ct image analysis. In *Proceedings of the IEEE/CVF International Conference on Computer Vision*, page 537–544, 2021. 1, 2
- [13] Dimitrios Kollias, Anastasios Arsenos, and Stefanos Kollias. Ai-mia: Covid-19 detection and severity analysis through medical imaging. In *European Conference on Computer Vision*, page 677–690. Springer, 2022. 2
- [14] Dimitrios Kollias, Anastasios Arsenos, and Stefanos Kollias. Ai-enabled analysis of 3-d ct scans for diagnosis of covid-19 & its severity. In *2023 IEEE International Conference on Acoustics, Speech, and Signal Processing Workshops (ICASSPW)*, page 1–5. IEEE, 2023. 1, 2
- [15] Dimitrios Kollias, Anastasios Arsenos, and Stefanos Kollias. A deep neural architecture for harmonizing 3-d input data analysis and decision making in medical imaging. *Neurocomputing*, 542:126244, 2023. 1, 3
- [16] Dimitrios Kollias, Anastasios Arsenos, James Wingate, and Stefanos Kollias. Sam2clip2sam: Vision language model for segmentation of 3d ct scans for covid-19 detection. *arXiv preprint arXiv:2407.15728*, 2024. 2, 3
- [17] Dimitrios Kollias, Anastasios Arsenos, and Stefanos Kollias. Pharos-afe-aimi: Multi-source & fair disease diagnosis. In *Proceedings of the IEEE/CVF International Conference on Computer Vision*, pages 7265–7273, 2025. 1, 2, 5, 6
- [18] Chia-Ming Lee, Bo-Cheng Qiu, Ting-Yao Chen, Ming-Han Sun, Fang-Ying Lin, Jung-Tse Tsai, I-An Tsai, Yu-Fan Lin, and Chih-Chung Hsu. Multi-source covid-19 detection via kernel-density-based slice sampling. *arXiv preprint arXiv:2507.01564*, 2025. 3, 5
- [19] Qingqiu Li, Runtian Yuan, Junlin Hou, Jilan Xu, Yuejie Zhang, Rui Feng, and Hao Chen. Advancing lung disease diagnosis in 3d ct scans. *arXiv preprint arXiv:2507.00993*, 2025. 3, 6
- [20] Tsung-Yi Lin, Priya Goyal, Ross Girshick, Kaiming He, and Piotr Dollár. Focal loss for dense object detection. In *Proceedings of the IEEE International Conference on Computer Vision (ICCV)*, pages 2980–2988, 2017. 2
- [21] Sachin Mehta and Mohammad Rastegari. Mobilevit: Lightweight, general-purpose, and mobile-friendly vision transformer. In *International Conference on Learning Representations (ICLR)*, 2022. Also available as arXiv:2110.02178. 1, 3
- [22] Shiori Sagawa, Pang Wei Koh, Tatsunori B. Hashimoto, and Percy Liang. Distributionally robust neural networks for group shifts: On the importance of regularization for worst-case generalization. In *International Conference on Learning Representations (ICLR)*, 2020. 1, 2, 3
- [23] Shiori Sagawa, Aditi Raghunathan, Pang Wei Koh, and Percy Liang. An investigation of why overparameterization exacerbates spurious correlations. In *International Conference on Machine Learning (ICML)*, 2020. 2
- [24] Q. Wang, F. Liu, R. Zou, et al. Enhancing medical image object detection with collaborative multi-agent deep q-networks and multi-scale representation. *EURASIP Journal on Advances in Signal Processing*, 2023(132):1–18, 2023. 2

- [25] Handan Xiao. 3d-2d medical image registration technology and its application development: a survey. In *Proceedings of the 2023 4th International Symposium on Artificial Intelligence for Medicine Science*, page 95–100, New York, NY, USA, 2024. Association for Computing Machinery. [2](#)
- [26] Jee Seok Yoon, Kwansook Oh, Yooseung Shin, Maciej A. Mazurowski, and Heung-II Suk. Domain generalization for medical image analysis: A review. *Proceedings of the IEEE*, 112(10):1583–1609, 2024. [2](#)
- [27] Runtian Yuan, Qingqiu Li, Junlin Hou, Jilan Xu, Yuejie Zhang, Rui Feng, and Hao Chen. Multi-source covid-19 detection via variance risk extrapolation. *arXiv preprint arXiv:2506.23208*, 2025. [3](#), [5](#)
- [28] Li Zhang, Xiaosong Wang, Dong Yang, Thomas Sanford, Stephanie Harmon, Baris Turkbey, Bradford J Wood, Holger Roth, Berengere Aubert-Broche, D Louis Collins, et al. Generalizing deep learning for medical image segmentation to unseen domains via deep stacked transformation. *IEEE Transactions on Medical Imaging*, 39(7):2531–2540, 2020. [1](#), [2](#)
- [29] Y. Zhang, P. Gu, N. Sapkota, and D. Z. Chen. Swipe: Efficient and robust medical image segmentation with implicit patch embeddings. In *Medical Image Computing and Computer Assisted Intervention – MICCAI 2023*, page 315–326, Cham, 2023. Springer. [3](#)
- [30] Zheyuan Zhang, Bin Wang, Lanhong Yao, Elif Keles, Debesh Jha, Matthew Antalek, Gorkem Durak, Alpay Medetalibeyoglu, Concetto Spampinato, Baris Turkbey, Boqing Gong, and Ulas Bagci. Adverin: Monotonic adversarial intensity attack for domain generalization in medical image segmentation. *Medical Image Analysis*, 107:103848, 2026. [2](#)